

Impact parameter profiles from nuclear shadowing ratio and applications to deuteron-gold collisions

Adeola Adeluyi,¹ Trang Nguyen,² and Bao-An Li¹

¹*Department of Physics and Astronomy*

Texas A&M University-Commerce, Commerce, TX 75429, USA

²*Center for Nuclear Research, Department of Physics*

Kent State University, Kent, OH 44242, USA

(Dated: November 10, 2018)

While current nuclear parton distribution functions (nPDFs) from global fits to experimental data are spatially homogeneous, many experimental observables in nucleus-nucleus collisions are presented in terms of centrality cuts. These cuts can be related to impact parameter using the Glauber theory and it is thus usual in the description of such observables to convolute an assumed impact parameter distribution with the homogeneous nPDFs. In this study we use the Gribov theory of nuclear shadowing supplemented with information from diffraction to model the impact parameter distributions of nuclear shadowing ratio in the small- x region. The modeled distributions are applied to the description of the centrality dependence of observables in deuteron-gold (d+Au) collisions at $\sqrt{s_{NN}} = 200$ AGeV.

PACS numbers: 24.85.+p, 25.30.Dh, 25.75.-q

I. INTRODUCTION

Nuclear parton distribution functions (nPDFs) encode the modifications to free nucleon parton distributions due to the complex, many-body environment in the nucleus. They are essential in the application of perturbative Quantum Chromodynamics (pQCD) to the description of many relevant observables in relativistic nucleus-nucleus collisions. Most of the currently available nPDFs [1–5] have been obtained from global fits to diverse experimental data. These nPDFs from global fits are homogeneous (independent of impact parameter), and are thus functions of the Bjorken variable x and squared momentum transferred Q^2 . An exception is [6] which is based on the Gribov theory [7] and available in both homogeneous and inhomogeneous forms.

Experimental data on nucleus-nucleus collisions are often presented in terms of centrality classes. These classes can be mapped into corresponding intervals in impact parameter space using the Glauber formalism. In order to adequately describe these data, inhomogeneous (impact-parameter-dependent) parton distributions are required. Due to the inherent constraints in the determination of nPDFs, especially in the gluon sector, it is pragmatic not to be limited in the choice of nPDF sets. Thus in order to take advantage of the different sets available, there is need for phenomenologically robust and realistic prescriptions for generating inhomogeneous nPDFs. This is usually carried out by convolution of impact parameter distributions with homogeneous nPDFs. One such prescription is given in [8] where two variants of impact parameter distributions are considered. The first variant assumes the distribution is proportional to the local nuclear density (generally taken as a Wood-Saxon nuclear density). The second takes the distribution as proportional to the nuclear path length (Glauber thick-

ness function). A simpler distribution is used in [9] where a hard sphere dependence is assumed.

Our objective in this study is to model impact parameter distributions which can be used with the homogeneous nPDFs in the spirit of [8, 10]. The general idea is to determine the impact parameter distributions which give a good description of the nuclear shadowing ratio in the region of small Bjorken x . These distributions are then applied in conjunction with a homogeneous nPDF set to calculate the centrality dependence of some observables in deuteron-gold collisions. A major simplification underlying the application is the assumption that the distributions derived from small- x shadowing are applicable to modifications at all values of x . As in [6, 11, 12] we employ a generalized form of the Gribov theory, incorporating the real part of the diffractive scattering amplitude. Experimental data for nuclear shadowing at small x are available from the NMC [13, 14] and E665 [15, 16] experiments. These experimental data are all at small Q^2 : thus the use of information from diffractive scattering of real photons ($Q^2 = 0$ GeV² at FNAL [17]) and quasi-real photons ($Q^2 < 0.01$ GeV² at HERA [18]) affords a good approximation.

In order to present a reasonably self-contained analysis, we include all the relevant details from our previous treatments. The paper is thus organized as follows: in Sec. II we review the basic formalism of Gribov theory as applied to shadowing in the small Bjorken- x regime. This section is essentially the same as in [12]. We present the results of our calculations for the shadowing ratio and the impact parameter distributions in Sec. III. In Sec. IV we illustrate a typical application of our results by using the distributions to describe the centrality dependence of the nuclear modification factor, pseudorapidity asymmetry, and hadron ratio in ultrarelativistic deuteron-gold (d+Au) collisions. We conclude in Sec. V.

II. NUCLEAR SHADOWING FROM GENERALIZED GRIBOV THEORY

A. Nuclear Shadowing Ratio

In nuclei, for small values of the Bjorken variable x ($x \lesssim 0.1$), the nuclear structure functions F_2^A are significantly reduced compared to the product of the mass number A and the free nucleon structure function F_2^N . Since the virtual photon-nucleus cross section is proportional to F_2 , then equivalently the virtual photon-nucleus cross section is less than A times the one for free nucleons, $\sigma_{\gamma^*A} < A \sigma_{\gamma^*N}$. This phenomenon is generally known as nuclear shadowing in the strict sense. Similar behavior is observed for real photons at sufficiently high energies ($\nu \gtrsim 3 \text{ GeV}$). Thus the nuclear shadowing ratio, defined as $F_2^A/(A * F_2^N)$ or alternatively as $\sigma_{\gamma^*A}/(A * \sigma_{\gamma^*N})$, is less than unity.

The (virtual) photon-nucleus cross section is separable into a part which accounts for the incoherent scattering from individual nucleons, and a correction (shadowing correction) from the coherent interaction with several nucleons:

$$\sigma_{\gamma^*A} = Z \sigma_{\gamma^*p} + (A - Z) \sigma_{\gamma^*n} + \delta\sigma_{\gamma^*A} \quad (1)$$

The single scattering part is the incoherent sum of photon-nucleon cross sections, where Z is the nuclear charge number, and σ_{γ^*p} and σ_{γ^*n} are the photon-proton and photon-neutron cross sections, respectively. The multiple scattering correction is expressible as an expansion in the number of nucleons in the target involved in the coherent scattering ($n \geq 2$). The dominant contribution to nuclear shadowing comes from double scattering, since the probability that the propagating hadronic excitation coherently interacts with several nucleons decreases with the number of nucleons.

We define the shadowing ratio as

$$\mathcal{R}_A^S = \frac{Z \sigma_{\gamma^*p} + (A - Z) \sigma_{\gamma^*n} + \delta\sigma_{\gamma^*A}}{Z \sigma_{\gamma^*p} + (A - Z) \sigma_{\gamma^*n}} \quad (2)$$

We neglect the small difference between the photon-proton cross section $\sigma_{\gamma p}$ and the photon-neutron cross section $\sigma_{\gamma n}$ in this study, and thus denote by σ_{γ^*N} the generic photon-nucleon cross section. The shadowing ratio can thus be written as

$$\mathcal{R}_A^S = 1 + \frac{\delta\sigma_{\gamma^*A}}{A \sigma_{\gamma^*N}} \quad (3)$$

Thus, the evaluation of the shadowing correction, $\delta\sigma_{\gamma^*A}$, is central to the calculation of the shadowing ratio. In the next section we utilize the Gribov theory in a generalized form to determine $\delta\sigma_{\gamma^*A}$.

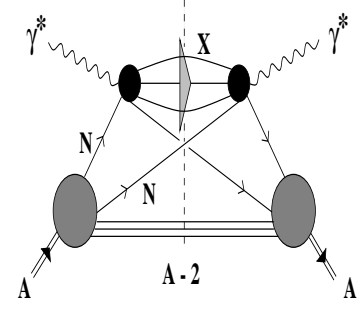


FIG. 1: Double scattering contribution to $\delta\sigma_{\gamma^*A}$.

B. Shadowing Correction From Generalized Gribov Theory

The original formulation of Gribov is generalized by including the real part of the diffractive scattering amplitude. We denote by η the ratio of the real to imaginary parts of the diffractive scattering amplitude. In this generalized form the shadowing correction at the level of double scattering is given by

$$\delta\sigma_{\gamma^*A} = \frac{A(A-1)}{2A^2} 16\pi \mathcal{R}e \left[\frac{(1-i\eta)^2}{1+\eta^2} \int d^2b \int_{-\infty}^{\infty} dz_1 \int_{z_1}^{\infty} dz_2 \int_{4m_\pi^2}^{W^2} dM_X^2 \frac{d^2\sigma_{\gamma^*N}^{\text{diff}}}{dM_X^2 dt} \Big|_{t \approx 0} \rho_A^{(2)}(\vec{b}, z_1; \vec{b}, z_2) \exp \left\{ i \frac{(z_1 - z_2)}{\lambda} \right\} \right] \quad (4)$$

with $\sigma_{\gamma^*N}^{\text{diff}}$ the photon-nucleon diffractive cross section. The coherence length, λ , is given by $\lambda = 2\nu/M_X^2$ for real photons. As illustrated in Fig. 1, a diffractive state with invariant mass M_X is produced in the interaction of the photon with a nucleon located at position (\vec{b}, z_1) in the target. The hadronic excitation is assumed to propagate at fixed impact parameter \vec{b} and to interact with a second nucleon at z_2 . The probability to find two nucleons in the target at the same impact parameter is described by the two-body density $\rho_A^{(2)}(\vec{b}, z_1; \vec{b}, z_2)$ normalized as $\int d^3r d^3r' \rho_A^{(2)}(\vec{r}, \vec{r}') = A^2$. The phase factor, $\exp \{i[(z_1 - z_2)/\lambda]\}$ in Eq. (4) implies that only diffractively excited hadrons with a longitudinal propagation length larger than the average nucleon-nucleon distance in the target, $\lambda > d \simeq 2 \text{ fm}$, can contribute significantly to double scattering. The limits of integration define the kinematically permitted range of diffractive excitations, with their invariant mass M_X above the two-pion production threshold and limited by the center-of-mass energy $W = \sqrt{s}$ of the scattering process.

We approximate the two-body density $\rho_A^{(2)}(\vec{b}, z_1; \vec{b}, z_2)$ by a product of one-body densities $\rho_A(\vec{r})\rho_A(\vec{r}')$ since short-range nucleon-nucleon correlations are relevant in nuclei only when $z_2 - z_1$ is comparable to the range of the

short-range repulsive part of the nucleon-nucleon force, i.e. for distances $\lesssim 0.4$ fm. However, shadowing is negligible in this case and therefore short-range correlations are not important in the shadowing domain.

With increasing photon energies or decreasing x down to $x \ll 0.1$, the longitudinal propagation length of diffractively excited hadrons rises and eventually reaches nuclear dimensions. Thus for heavy nuclei, interactions of the excited hadronic state with several nucleons in the target become important and should be accounted for. Following [6] we introduce an attenuation factor with an effective hadron-nucleon cross section, σ_{eff} . The shadowing correction can thus be written as

$$\delta\sigma_{\gamma^*A} = \frac{A(A-1)}{2A^2} 16\pi \text{Re} \left[\frac{(1-i\eta)^2}{1+\eta^2} \int d^2b \int_{-\infty}^{\infty} dz_1 \int_{z_1}^{\infty} dz_2 \int_{4m_\pi^2}^{W^2} dM_X^2 \frac{d^2\sigma_{\gamma^*N}^{\text{diff}}}{dM_X^2 dt} \Big|_{t \approx 0} \rho_A^{(2)}(\vec{b}, z_1; \vec{b}, z_2) \exp \left\{ i \frac{(z_1 - z_2)}{\lambda} \right\} \exp \left\{ -(1/2)(1-i\eta)\sigma_{\text{eff}} \int_{z_1}^{z_2} dz \rho_A(b, z) \right\} \right] \quad (5)$$

The effective hadron-nucleon cross section, σ_{eff} in Eq. (5) is defined as

$$\sigma_{\text{eff}} = \frac{16\pi}{\sigma_{\gamma N}(1+\eta^2)} \int_{4m_\pi^2}^{W^2} dM_X^2 \frac{d^2\sigma_{\gamma^*N}^{\text{diff}}}{dM_X^2 dt} \Big|_{t \approx 0} \quad (6)$$

where $\sigma_{\gamma N}$ is the photon-nucleon cross section. The details of this approach and the approximations inherent in the definition of σ_{eff} are treated thoroughly in [6]. For vector mesons as the intermediate hadronic excitations, we take σ_{VN} as σ_{eff} in the attenuation factor in Eq. (5), where σ_{VN} is the vector meson-nucleon scattering cross section.

C. Impact Parameter Profile

The shadowing correction (5) can be expressed as

$$\delta\sigma_{\gamma^*A} = \int d^2b \mathcal{F}_A^S(b) , \quad (7)$$

where

$$\mathcal{F}_A^S(b) = \frac{(A-1)}{A^2 \sigma_{\gamma^*N}} 8\pi \text{Re} \left[\frac{(1-i\eta)^2}{1+\eta^2} \int_{-\infty}^{\infty} dz_1 \int_{z_1}^{\infty} dz_2 \int_{4m_\pi^2}^{W^2} dM_X^2 \frac{d^2\sigma_{\gamma^*N}^{\text{diff}}}{dM_X^2 dt} \Big|_{t \approx 0} \rho_A^{(2)}(\vec{b}, z_1; \vec{b}, z_2) \exp \left\{ i \frac{(z_1 - z_2)}{\lambda} \right\} \exp \left\{ -(1/2)(1-i\eta)\sigma_{\text{eff}} \int_{z_1}^{z_2} dz \rho_A(b, z) \right\} \right] \quad (8)$$

We make use of the fact that the shadowing correction, $\delta\sigma_{\gamma^*A}$, is a real number and write

$$\int db \frac{2\pi b \mathcal{F}_A^S(b)}{\delta\sigma_{\gamma^*A}} = \int db \mathcal{G}_A^S(b) = 1 , \quad (9)$$

which is reminiscent of the thickness function distribution:

$$\int db \frac{2\pi b \int dz \rho_A(\vec{b}, z)}{A} = 1 . \quad (10)$$

The integrands in Eq. (9) and Eq. (10) for both light and heavy nuclei are shown in Sec. III.

D. Diffractive Dissociation

The shadowing correction, $\delta\sigma_{\gamma^*A}$, which is the major component in the evaluation of the shadowing ratio and impact parameter profile, involves the differential diffractive dissociation cross section. The determination of this cross section is the subject of this section.

The analysis by the H1 Collaboration[18] divides the HERA diffractive dissociation data into effectively three intervals in M_X^2 : the first interval (0.16 – 1.58) GeV² contains the region of the low-mass vector mesons (ρ , ω and ϕ), the second interval (1.58 – 4.0 GeV²) covers the ρ' resonance region, while the third interval ($M_X^2 > 4.0$ GeV²) is that of the high-mass continuum. Due to the similarity in the theoretical description of the first and second intervals, we combine them together. The differential diffractive cross section is thus written as a sum over contributions from two mass intervals,

$$\frac{d\sigma_{\gamma N}^D}{dM_X^2 dt} \Big|_{t \approx 0} = \sum_{V=\rho, \omega, \phi, \rho'} \frac{d\sigma_{\gamma N}^V}{dM_X^2 dt} \Big|_{t \approx 0} + \frac{d\sigma_{\gamma N}^{\text{cont}}}{dM_X^2 dt} \Big|_{t \approx 0} \quad (11)$$

In the following, we briefly summarize the various approximations applied in these intervals.

1. Low-mass vector mesons and the ρ' resonances

We utilize the generalized vector meson dominance (VMD) [19] to describe the contribution of the low-mass vector mesons to the differential diffractive cross section:

$$\frac{d\sigma_{\gamma N}^V}{dM_X^2 dt} \Big|_{t \approx 0} = \frac{e^2}{16\pi} \frac{\Pi^V(M_X^2)}{M_X^2} \sigma_{VN}^2 \quad (12)$$

with $\Pi^V(M_X^2)$ the vector meson part of the photon spectral function $\Pi(M_X^2)$, which is given by

$$\Pi(M_X^2) = \frac{1}{12\pi^2} \frac{\sigma(e^+e^- \rightarrow \text{hadrons})}{\sigma(e^+e^- \rightarrow \mu^+\mu^-)} \quad (13)$$

In Eq. (12), σ_{VN} is the vector meson-nucleon cross section and $e^2/4\pi = 1/137$ is the fine structure constant.

The ω and ϕ mesons are narrow and thus well approximated by delta functions. Their contribution to the photon spectral function can be written as

$$\Pi^V(M_X^2) = \left(\frac{m_V}{g_V}\right)^2 \delta(M_X^2 - m_V^2) \quad ; \quad V = \omega, \phi, \quad (14)$$

where m_V and g_V , ($V = \omega, \phi$) are the mass and the coupling constant of the ω and ϕ mesons, respectively.

The ρ -meson, unlike the ω and ϕ mesons, has a large width due to its strong coupling to two-pion states. We have followed the approach in [20] and taken this into account through the $\pi^+\pi^-$ part of the photon spectral function:

$$\Pi^\rho(M_X^2) = \frac{1}{48\pi^2} \Theta(M_X^2 - 4m_\pi^2) \left(1 - \frac{4m_\pi^2}{M_X^2}\right)^{3/2} |F_\pi(M_X^2)|^2, \quad (15)$$

where m_π is the mass of the pion and $M_X = M_{\pi\pi}$ is the invariant mass of the $\pi^+\pi^-$ pair. The pion form factor, F_π is taken from Ref. [21]. A full discussion is given in [20]. We compared the result from the delta function approximation to this more exact calculation and found that taking into account the width of the ρ -meson increases the differential diffractive cross section by about 10%.

The ρ' resonance region contains the $\rho(1450)$ and $\rho(1700)$ mesons which were formerly classified as the $\rho(1600)$ [22]. The FNAL data show an enhancement in this region and we treat this enhancement in terms of an average ρ' resonance, corresponding to the earlier classification of $\rho(1600)$, as done in Ref. [17]. We use the available information on the $\rho(1600)$ from Ref. [19] in a VMD-type calculation to evaluate the contribution from this region. The average ρ' resonance should have a finite width, but encouraged by the fact that a delta function in the case of the ρ gives a good approximation to the full-width result, we employ a narrow resonance approximation for the $\rho(1600)$:

$$\left.\frac{d\sigma_{\gamma N}^V}{dM_X^2 dt}\right|_{t \approx 0} = \frac{e^2}{16\pi} \frac{\Pi^V(M_X^2)}{M_X^2} \sigma_{VN}^2 \quad (16)$$

with

$$\Pi^V(M_X^2) = \left(\frac{m_V}{g_V}\right)^2 \delta(M_X^2 - m_V^2) \quad (17)$$

and $V = \rho(1600)$.

2. High-mass continuum

A full treatment of both the FNAL data and the HERA data in this region has been carried out by the H1 Collaboration in Ref. [18], using the triple-Regge model of photon dissociation. Here we consider

only the aspects relevant to the present study. There are two diffractive terms in the triple-Regge expansion: the triple-pomeron ($\mathbb{P}\mathbb{P}\mathbb{P}$) and the pomeron-pomeron-reggeon ($\mathbb{P}\mathbb{P}\mathbb{R}$) terms. The subleading reggeons have the quantum numbers of the ρ , ω , a_2 and f_2 mesons and their trajectories are approximately degenerate. They are generally referred to as ρ , ω , a and f mesons and their isospin, signature and C - and G - parities are $\rho(1 - -)$, $\omega(0 - -)$, $a(1 + +)$ and $f(0 + +)$. The pomeron has $\mathbb{P}(0 + +)$ and is thus identical to the f meson, leading to interference. We neglect such interference effect in the present study.

The differential dissociation cross section can thus be written as

$$\frac{d^2\sigma}{dM_X^2 dt} = \left[\frac{G_{\mathbb{P}\mathbb{P}\mathbb{P}}(0)}{M_X^{2\alpha_{\mathbb{P}}(0)}} + \frac{G_{\mathbb{P}\mathbb{P}\mathbb{R}}(0)}{M_X^{4\alpha_{\mathbb{P}}(0) - 2\alpha_{\mathbb{R}}(0)}} \right] (W^2)^{2\alpha_{\mathbb{P}}(0) - 2} e^{B(W^2, M_X^2)t}, \quad (18)$$

where $B(W^2, M_X^2) = 2b_{p\mathbb{P}} + 2\alpha'_{\mathbb{P}} \ln(W^2/M_X^2)$ and $b_{p\mathbb{P}}$ is the proton-pomeron slope parameter. $\alpha'_{\mathbb{P}}$ is the slope of the pomeron trajectory while $\alpha_{\mathbb{P}}$ and $\alpha_{\mathbb{R}}$ are the pomeron and (effective) reggeon intercept respectively. We use the values in [18] for these parameters. Note that the value of $\alpha_{\mathbb{P}}(0)$ ($\alpha_{\mathbb{P}}(0) = 1.068 \pm 0.0492$) agrees within error with the soft pomeron intercept in Ref. [23] ($\alpha_{\mathbb{P}}(0) \simeq 1.081$). The usual triple-pomeron approximation corresponds to putting $G_{\mathbb{P}\mathbb{P}\mathbb{R}}(0) = 0$ in Eq. (18). The contributions from the subleading reggeons are small at both NMC and E665 energies [12], thus we use the triple-pomeron approximation in this study. We use the value of $G_{\mathbb{P}\mathbb{P}\mathbb{P}}(0) = 9.0$ from the analysis in [12].

III. RESULT: SHADOWING RATIO AND IMPACT PARAMETER PROFILE

The treatment outlined in the last section is now applied to calculate the shadowing ratio and the impact parameter profile. The basic expression is Eq. (8), which involves the ratio of the real to imaginary amplitudes η , the photon-nucleon cross section $\sigma_{\gamma N}$, the nuclear density ρ_A , and the effective cross section σ_{eff} in terms of the diffractive dissociation cross section.

We use the energy-independent η 's for the vector mesons from Ref. [19]. For both ρ and ω mesons, η takes values between 0 and -0.3 . Here we take $\eta_\rho = \eta_\omega = -0.2$ in accordance with Ref. [19]. The results of our calculation are not very sensitive to the precise values of $\eta_{\rho(\omega)}$. For the ϕ meson, we take $\eta_\phi = 0.13$ [24]. Due to lack of information, we take $\eta_{\rho(1600)} = 0$. For the high-mass continuum, we follow Ref. [6] and define $\eta_{\mathbb{P}}$ as

$$\eta_{\mathbb{P}} = \frac{\pi}{2} (\alpha_{\mathbb{P}}(0) - 1), \quad (19)$$

using the result of Gribov and Migdal [25].

We use the Donnachie-Landshoff parameterization of $\sigma_{\gamma p}$ [23] as the generic photon-nucleon cross section $\sigma_{\gamma N}$.

For the nuclear densities three-parameter Fermi ($3pF$) distributions are applied:

$$\rho(r) = \rho_0 \frac{1 + \omega(r/R_A)^2}{1 + e^{(r-R_A)/d}}, \quad (20)$$

with the parameter values taken from Ref. [26]. For mass numbers $A \lesssim 20$ a harmonic oscillator (HO) density distribution may be more appropriate than the $3pF$ distribution. For uniformity, we use the $3pF$ distributions for the whole mass range in light of the fact that uncertainties associated with other parameters are at least comparable.

A. Shadowing Ratio At Small x

At very small x ($x \simeq 10^{-4}$) the E665 experiment has four data points: ^{12}C , ^{40}Ca , ^{131}Xe , and ^{208}Pb . The results of our calculation and the experimental data are shown in Fig. 2. For small A the shadowing ratio decreases rapidly with A , while for large A the decrease is more gradual. The result is in good agreement with experiment, and reproduces quite accurately the trend of the small x shadowing with mass number A .

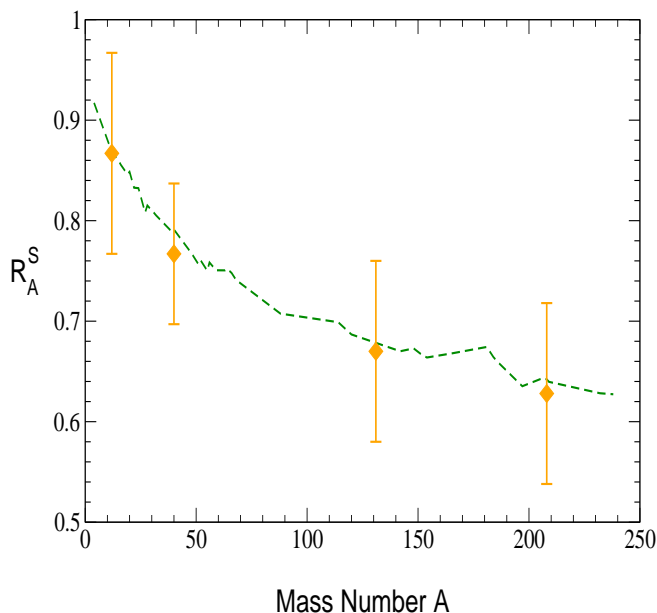


FIG. 2: (Color Online) Shadowing ratio at small x . The dashed curve is the result of our calculation. The shaded triangles are data from the E665 experiment.

B. Impact Parameter Profile At Small x

We use Eq. (9) to determine the impact parameter profile for nuclei in the mass range $3 < A < 239$ and at small x ($x \simeq 10^{-4}$). In Fig. 3 we present the profile as a function of impact parameter b for four representative nuclei: ^{12}C , ^{63}Cu , ^{197}Au , and ^{208}Pb . These results are shown in the figure as solid curves.

As noted in the introduction, two prescriptions are given in [8]: a local density dependence and a Glauber thickness function scaling. At small Bjorken- x the thickness function dependence is probably more physical. Its impact parameter distribution, from Eq. (10), is shown as dashed curves in Fig. 3. For both the shadowing cor-

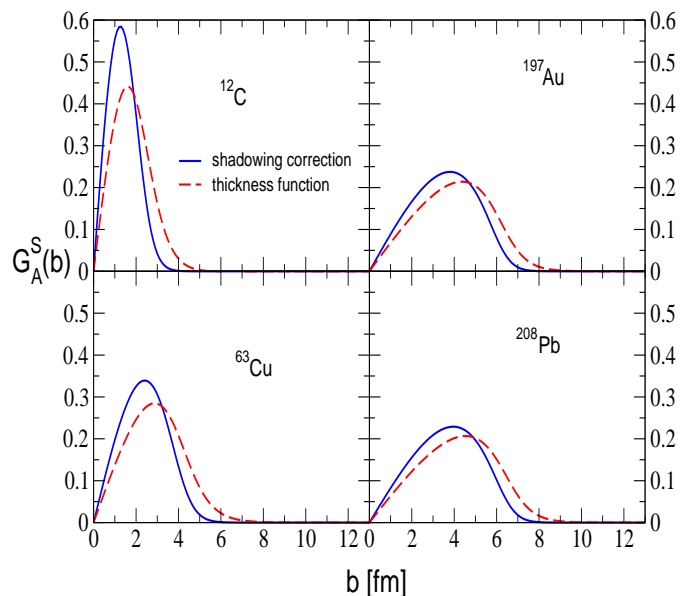


FIG. 3: (Color Online) Impact parameter profile at small x . The solid and dashed curves are the results from the present study and thickness function dependence respectively.

rection and thickness function, the profiles have narrow widths and sharp peaks for light nuclei, with the widths and peaks broadening out as the mass number increases. Since the profiles are normalized to unity, it is easy to see their differences: the profiles from the shadowing correction have taller peaks and a steeper dropoff to zero than those from the thickness function dependence.

Fig. 3 only shows the profiles as a function of b for four nuclei. In Fig. 4 we show the full result of our calculation of the profile from shadowing correction as a function of both the mass number A and impact parameter b . The features noted in the preceding paragraph are clearly manifested.

A. Collinear factorization

The cross section for the $d+Au \rightarrow h+X$ reaction, with respect to pseudorapidity η and transverse momentum p_T can be written as

$$\frac{d\sigma_{dAu}^h}{d\eta d^2p_T} = \sum_{abcd} \int d^2b d^2s dx_a dx_b dz_c t_d(\vec{s}) t_{Au}(|\vec{b}-\vec{s}|) F_{a/d}(x_a, Q^2, \vec{s}, z) F_{b/Au}(x_b, Q^2, |\vec{b}-\vec{s}|, z') \frac{d\sigma(ab \rightarrow cd)}{d\hat{t}} \frac{D_{h/c}(z_c, Q_f^2)}{\pi z_c^2} \hat{s} \delta(\hat{s} + \hat{t} + \hat{u}) \quad (23)$$

where x_a and x_b are parton momentum fractions in deuteron and gold, respectively, and z_c is the fraction of the parton momentum carried by the final-state hadron h . The factorization and fragmentation scales are Q and Q_f respectively. Here

$$t_A(\vec{s}) = \int dz \rho_A(\vec{s}, z) \quad (24)$$

is the Glauber thickness function of nucleus A , with the nuclear density distribution, $\rho_A(\vec{s}, z)$ subject to the normalization condition

$$\int d^2s dz \rho_A(\vec{s}, z) = A. \quad (25)$$

The quantity $d\sigma(ab \rightarrow cd)/d\hat{t}$ in Eq. (23) represents the perturbatively calculable partonic cross section, and $D_{h/c}(z_c, Q_f^2)$ stands for the fragmentation function of parton c to produce hadron h , evaluated at momentum fraction z_c and fragmentation scale Q_f .

Since we are interested in the description of centrality-selected data using nPDFs which are spatially homogeneous, we need to incorporate some form of impact parameter dependency. We follow the approach in [8, 10] and write

$$F_{a/A}(x, Q^2, \vec{s}, z) = f_{a/N}(x, Q^2) S(A, x, Q^2, \vec{s}, z). \quad (26)$$

Here $f_{a/N}(x, Q^2)$ is the nucleon parton distribution function, which can be expressed as

$$f_{a/N}(x, Q^2) = \frac{Z}{A} f_{a/p}(x, Q^2) + (1 - \frac{Z}{A}) f_{a/n}(x, Q^2), \quad (27)$$

with $f_{a/p}(x, Q^2)$ ($f_{a/n}(x, Q^2)$) being the proton (neutron) parton distribution function as a function of Bjorken x and factorization scale Q . The inhomogeneous shadowing function is defined as

$$S(A, x, Q^2, \vec{s}, z) = 1 + N_\Phi [S'(A, x, Q^2) - 1] \Phi(\vec{s}, z) \quad (28)$$

with $\Phi(\vec{s}, z)$ dimensionless and N_Φ a suitable normalization constant such that

$$\frac{1}{A} \int d^2s dz \rho_A(\vec{s}, z) S(A, x, Q^2, \vec{s}, z) = S'(A, x, Q^2) \quad (29)$$

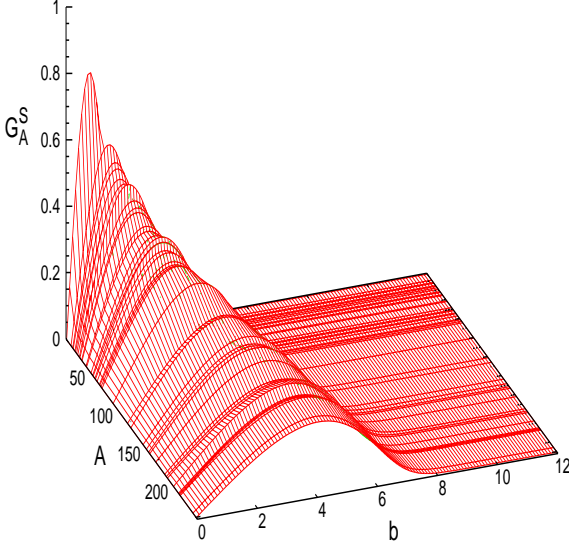


FIG. 4: (Color On line) Impact parameter profile at small x as a function of mass number A and impact parameter b .

For applications to deuteron-gold collisions (Sec. IV) it is convenient to define the dimensionless form of the impact parameter distribution. A suitable form for the shadowing correction (sc) is

$$\mathcal{W}_A^{sc}(b) = \frac{\mathcal{F}_A^S(b)}{\mathcal{F}_A^S(0)} \quad (21)$$

while for the thickness function (tf) we can define

$$\mathcal{W}_A^{tf}(b) = \frac{\int dz \rho_A(\vec{b}, z)}{\int dz \rho_A(0, z)}. \quad (22)$$

These forms are not unique: any suitable value of b can be used in the denominator to render the profiles dimensionless.

IV. APPLICATION TO DEUTERON-GOLD (D+AU) COLLISIONS

We now apply the impact parameter profile discussed in Sec. IIIB to calculate the centrality dependence of some observable quantities in deuteron-gold collisions: nuclear modification factor for π^0 , $R_{dAu}^{\pi^0}$, pseudorapidity asymmetry, Y_{Asy} , for pions and protons, and hadron-to-pion ratio.

Here $S'(A, x, Q^2)$ denotes the homogeneous shadowing function. Note that the homogeneous nPDFs are the product of the homogeneous shadowing function $S'(A, x, Q^2)$ and the nucleonic PDFs $f_{a/N}(x, Q^2)$. The dimensionless function $\Phi(\vec{s}, z)$ furnishes the required impact parameter dependency. We use the profile derived from the shadowing correction, $\mathcal{W}_A^{sc}(b)$ (Eq. (21)), subject to the normalization condition in Eq. (29).

The density distribution of the deuteron is obtained from the Hulthen wave function[27] (as in Ref. [28]), while the density distribution for gold is taken as a Woods-Saxon distribution with parameters from Ref. [26]. We fix the scales as $Q = Q_f = p_T$, where p_T is the transverse momentum of the final hadron. The partonic differential cross sections, $d\sigma(ab \rightarrow cd)/d\hat{t}$ were evaluated at leading order (LO). We note that, if a K factor was used to approximate the effects of higher orders, these effects would cancel in the ratios calculated in the present study. We use the Eskola-Paukkunen-Salgado (EPS08)[2] shadowing functions with the MRST2001 leading order (LO) parton distribution functions (PDFs)[29]. For the fragmentation functions we use the DSS set [30, 31] for pions and protons.

As stated earlier experimental data are often presented in terms of centrality classes, the most central class corresponding to head-on collisions. The Glauber description of heavy ion collisions afford a connection between centrality classes and impact parameter cuts. An analytic expression valid to a very good approximation is given by [32]

$$c \approx \frac{\pi b^2}{\sigma_{dAu}^{inel}} \quad (30)$$

where c is the centrality, b the impact parameter, and σ_{dAu}^{inel} is the inelastic deuteron-gold cross section.

B. Nuclear Modification Factor

The d+Au nuclear modification factor for a hadron h , R_{dAu}^h , is defined as

$$R_{dAu}^h(p_T) = \frac{1}{\langle N_{bin} \rangle} \frac{d\sigma_{dAu}^h}{d\eta d^2p_T} \bigg/ \frac{d\sigma_{pp}^h}{d\eta d^2p_T}, \quad (31)$$

where the average number of binary collisions, $\langle N_{bin} \rangle$ in the various impact-parameter bins is given by

$$\langle N_{bin} \rangle = \langle \sigma_{NN}^{inel} T_{dAu}(b) \rangle. \quad (32)$$

Here σ_{NN}^{inel} is the inelastic nucleon-nucleon cross section and

$$T_{dAu}(b) = \int d^2s t_d(\vec{s}) t_{Au}(|\vec{b} - \vec{s}|) \quad (33)$$

represents the deuteron-gold nuclear overlap function. The nuclear modification factor R_{dAu}^h is thus just the

ratio of the d+Au and proton-proton (pp) cross sections, normalized by the average number of binary collisions, $\langle N_{bin} \rangle$.

The PHENIX Collaboration has presented results for the nuclear modification factor for neutral pions [33] in the pseudorapidity interval $|\eta| < 0.35$ and four centrality classes: 0 – 20%, 20 – 40%, 40 – 60%, and 60 – 88%. We use these classes and the results of our calculations are displayed in Fig. 5, together with the experimental data.

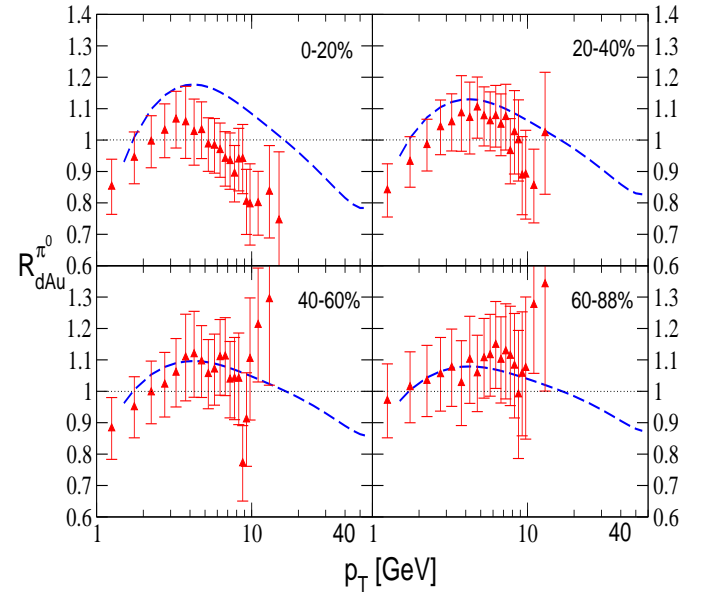


FIG. 5: (Color Online) Nuclear modification factor R_{dAu} for neutral pion in different centrality classes. Filled triangles denote experimental data from the PHENIX Collaboration [33].

Our calculation overshoots the data for the central class (0 – 20%). This is in part a reflection of the fact that the minimum bias EPS08 overpredicts the data by about 5%. The data shows the influence of shadowing ($R_{dAu}^{\pi^0} < 1$) for $p_T < 2.5$ GeV, antishadowing ($R_{dAu}^{\pi^0} > 1$) for $2.5 < p_T < 6$ GeV, and the EMC effect ($R_{dAu}^{\pi^0} < 1$) for $p_T > 6$ GeV. While our calculation follows this general trend, the data shows a narrower window for the antishadowing peak relative to calculation. Away from the central class, the antishadowing peak progressively broadens with increasing centrality, and this is adequately reproduced by calculation. The agreement with data is in fact quite reasonable for the other centrality classes under consideration.

C. Pseudorapidity Asymmetry

As the mechanisms for hadron production in d+Au collisions may be different at forward rapidities (deuteron side) and backward rapidities (gold side), it is of interest to study ratios of particle yields between a given rapidity value and its negative in these collisions. The STAR Collaboration has measured pseudorapidity asymmetries, defined as

$$Y_{Asy} = \frac{d\sigma_{dAu}^h}{d\eta d^2p_T}(\text{Au-side}) / \frac{d\sigma_{dAu}^h}{d\eta d^2p_T}(\text{d-side}) , \quad (34)$$

in d+Au collisions for several identified hadron species and total charged hadrons in the pseudorapidity intervals $|\eta| \leq 0.5$ and $0.5 \leq |\eta| \leq 1.0$ [34]. Here we consider the pseudorapidity asymmetry for both pions and protons in different centrality classes for the two STAR pseudorapidity intervals.

Fig. 6 shows the result of our calculation of the pseudorapidity asymmetry for pions (upper panels) and protons (lower panels) for the interval $|\eta| \leq 0.5$ and centralities 0 – 20% and 40 – 100% respectively. For the pions, our

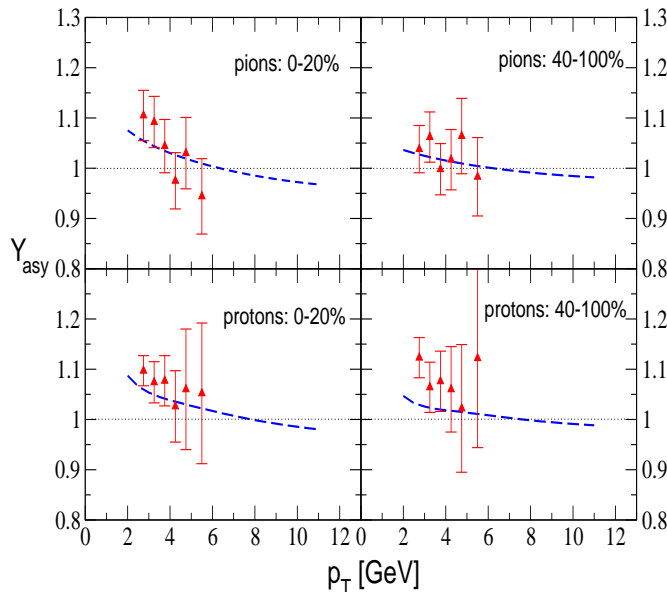


FIG. 6: (Color Online) Centrality dependence of pseudorapidity asymmetry for pions (upper panels) and protons (lower panels) in the interval $|\eta| \leq 0.5$. Filled triangles denote experimental data from the STAR Collaboration [34].

calculations are in good agreement with data for both centrality classes, especially for the 40 – 100% (peripheral) class where the agreement is manifestly excellent. In the case of protons, the calculation reproduces the

data very well for the 0 – 20% (central) class. It is off by a few percent for the peripheral class.

Two general remarks are in order: first, the magnitude of the pseudorapidity asymmetry is rather small in this interval, generally less than or of the order of 10%. This is manifested both by experiment and calculation, and is due to the fact that the considered interval is close to midrapidity. Second, the calculation exhibits a greater degree of asymmetry for the central class relative to the peripheral.

The result of our calculation for the pseudorapidity interval $0.5 \leq |\eta| \leq 1.0$ is presented in Fig. 7. Away from midrapidity, the asymmetry is appreciably enhanced and this is reflected by both experiment and calculation. Also, as observed in the previous interval, the magnitude of the asymmetry decreases with increasing centrality. Overall, the agreement with data is manifestly good for both pions and protons and in both central and peripheral classes.

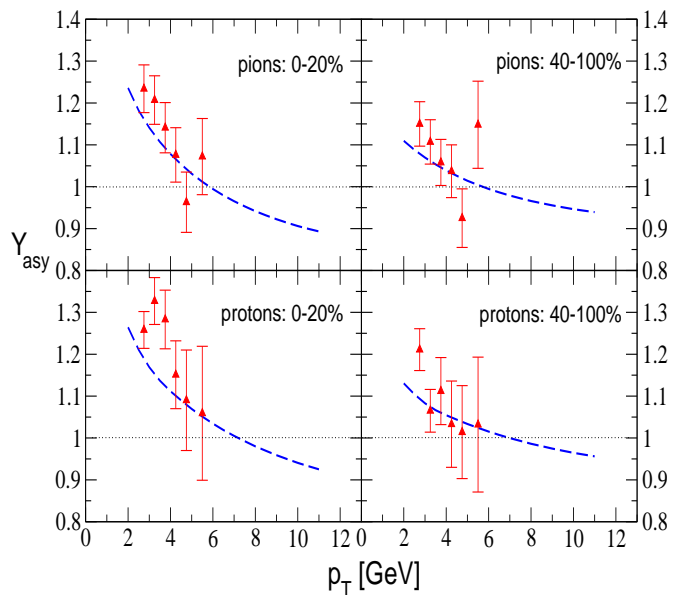


FIG. 7: (Color Online) Centrality dependence of pseudorapidity asymmetry for pions (upper panels) and protons (lower panels) in the interval $0.5 \leq |\eta| \leq 1.0$. Filled triangles denote experimental data from the STAR Collaboration [34].

D. Hadron Ratio

As a final example of the application of the impact parameter profile to d+Au collisions, we consider the centrality dependence of the ratio of hadrons to pions, as

measured by the PHENIX Collaboration [35]. We denote this ratio as $\mathcal{R}_{dAu}^{h/\pi}$ and write

$$\mathcal{R}_{dAu}^{h/\pi}(p_T) = \frac{d\sigma_{dAu}^{(h^++h^-)/2}}{d\eta d^2p_T} \bigg/ \frac{d\sigma_{dAu}^{\pi^0}}{d\eta d^2p_T}. \quad (35)$$

The centrality classes are the same as for the π^0 nuclear modification factor, viz: 0 – 20%, 20 – 40%, 40 – 60%, and 60 – 88%. Fig. 8 shows the result of our calculation for these four centrality classes. The trend also mirrors that observed for $R_{dAu}^{\pi^0}$. Our calculations overshoot the

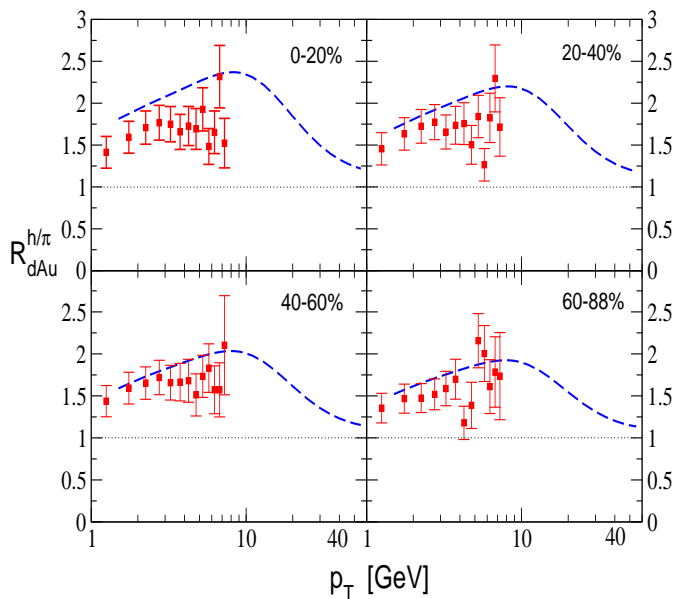


FIG. 8: (Color Online) Centrality dependence of hadron-to-pion ratio. Filled squares denote experimental data from the PHENIX Collaboration [35].

data for the most central class (0 – 20%) especially at higher p_T . The agreement with data is more reasonable for the other centrality classes.

V. CONCLUSION

We have calculated the the shadowing ratio and impact parameter profiles for nuclei in the mass range

$3 < A < 240$ and for small x ($x \simeq 10^{-4}$) using a suitably generalized form of the Gribov theory. The photon diffractive dissociation cross section, which is the main input to our calculation, has been parameterized as a function of the invariant mass of the diffractively produced hadronic excitation in two effective mass intervals. For the low-mass vector mesons and ρ' resonances, vector meson dominance model is used while the high-mass continuum is treated within the framework of triple-Regge theory. Relevant model parameters are taken from experiments and earlier studies.

The calculated result for the shadowing ratio agrees nicely with small x shadowing data from the E665 experiment and also reproduces quite well the trend of shadowing with mass number A . We compare the resultant impact parameter profiles for four representative nuclei with the Glauber thickness function dependence which has been previously applied in the literature. We also present the profiles as a function of both mass number A and impact parameter b for $3 < A < 240$ and $0 < b < 12$ fm.

We illustrate the utility of the impact parameter distributions by applying them to calculate the centrality dependence of three different observables in deuteron-gold collisions: the π^0 nuclear modification factor $R_{dAu}^{\pi^0}$, pseudorapidity asymmetry Y_{Asy} for pions and protons, and the hadron-to-pion ratio, $\mathcal{R}_{dAu}^{h/\pi}$. Except for the overshoot at the most central class, our calculation gives an adequate description of the centrality behavior of both $R_{dAu}^{\pi^0}$ and $\mathcal{R}_{dAu}^{h/\pi}$ as measured by the PHENIX Collaboration. The agreement with the STAR data for the centrality dependence of pseudorapidity asymmetry is also good for both pions and protons. This is encouraging considering the fact that the distributions have been derived from the small- x shadowing ratio, and thus in a strict sense reflects the behavior in the shadowing region, i.e. $x < 0.1$.

VI. ACKNOWLEDGMENT S

This work was supported in part by the NSF grant PHY0757839.

[1] K. J. Eskola, H. Paukkunen and C. A. Salgado, JHEP **0904**, 065 (2009)

[2] K. J. Eskola, H. Paukkunen and C. A. Salgado, JHEP **0807**, 102 (2008)

- [3] K. J. Eskola, V. J. Kolhinen and C. A. Salgado, *Eur. Phys. J. C* **9**, 61 (1999).
- [4] M. Hirai, S. Kumano, and T.-H. Nagai, *Phys. Rev. D* **70**, 044905 (2004); *Nucl. Phys. B Proc. Suppl.* **139**, 21 (2005).
- [5] D. de Florian and R. Sassot, *Phys. Rev. D* **69**, 074028 (2004).
- [6] L. Frankfurt, V. Guzey and M. Strikman, *Phys. Rev. D* **71**, 054001 (2005); *Phys. Lett. B* **586**, 41 (2004).
- [7] V. N. Gribov, *Sov. Phys. JETP* **30**, 709 (1970) [*Zh. Eksp. Teor. Fiz.* **57**, 1306 (1969)].
- [8] R. Vogt, *Phys. Rev. C* **70**, 064902 (2004).
- [9] S. y. Li and X. N. Wang, *Phys. Lett. B* **527**, 85 (2002).
- [10] A. Adeluyi and G. I. Fai, *Phys. Rev. C* **76**, 054904 (2007).
- [11] A. Adeluyi and G. Fai, *Phys. Rev. C* **74**, 054904 (2006).
- [12] A. Adeluyi and T. Nguyen, *Phys. Rev. C* **75**, 054911 (2007).
- [13] P. Amaudruz *et al.* [New Muon Collaboration], *Nucl. Phys. B* **441**, 3 (1995).
- [14] M. Arneodo *et al.* [New Muon Collaboration.], *Nucl. Phys. B* **441**, 12 (1995).
- [15] M. R. Adams *et al.* [E665 Collaboration], *Phys. Rev. Lett.* **68**, 3266 (1992).
- [16] M. R. Adams *et al.* [E665 Collaboration], *Z. Phys. C* **67**, 403 (1995).
- [17] T. J. Chapin *et al.*, *Phys. Rev. D* **31**, 17 (1985).
- [18] C. Adloff *et al.* [H1 Collaboration], *Z. Phys. C* **74**, 221 (1997).
- [19] T. H. Bauer, R. D. Spital, D. R. Yennie and F. M. Pipkin, *Rev. Mod. Phys.* **50**, 261 (1978) [Erratum-ibid. **51**, 407 (1979)].
- [20] G. Piller, G. Niesler and W. Weise, *Z. Phys. A* **358**, 407 (1997).
- [21] F. Klingl, N. Kaiser and W. Weise, “Effective Lagrangian approach to vector mesons, their structure and *Z. Phys. A* **356**, 193 (1996).
- [22] K. Hagiwara *et al.* [Particle Data Group], *Phys. Rev. D* **66**, 010001 (2002).
- [23] A. Donnachie and P. V. Landshoff, *Phys. Lett. B* **296**, 227 (1992).
- [24] L. Frankfurt, G. Piller, M. Sargsian and M. Strikman, *Eur. Phys. J. A* **2**, 301 (1998).
- [25] V. N. Gribov and A. A. Migdal, *Sov. J. Nucl. Phys.* **8**, 583 (1969) [*Yad. Fiz.* **8**, 1002 (1968)].
- [26] C. W. De Jager, H. De Vries and C. De Vries, *Atom. Data Nucl. Data Tabl.* **14**, 479 (1974).
- [27] L. Hulthen and M. Sugawara, “Handbuch der Physik”, vol. 39 (1957).
- [28] D. Kharzeev, E. Levin and M. Nardi, *Nucl. Phys. A* **730**, 448 (2004) [Erratum-ibid. **A 743**, 329 (2004)].
- [29] A. D. Martin, R. G. Roberts, W. J. Stirling and R. S. Thorne, *Eur. Phys. J. C* **23**, 73 (2002).
- [30] D. de Florian, R. Sassot and M. Stratmann, *Phys. Rev. D* **75**, 114010 (2007) [arXiv:hep-ph/0703242].
- [31] D. de Florian, R. Sassot and M. Stratmann, *Phys. Rev. D* **76**, 074033 (2007) [arXiv:0707.1506 [hep-ph]].
- [32] W. Broniowski and W. Florkowski, *Phys. Rev. C* **65**, 024905 (2002).
- [33] S. S. Adler *et al.* [PHENIX Collaboration], *Phys. Rev. Lett.* **98**, 172302 (2007).
- [34] B. I. Abelev *et al.* [STAR Collaboration], *Phys. Rev. C* **76**, 054903 (2007); J. Adams *et al.* [STAR Collaboration], *Phys. Rev. C* **70**, 064907 (2004).
- [35] S. S. Adler *et al.* [PHENIX Collaboration], *Phys. Rev. C* **77**, 014905 (2008).